

Ill-posed formulation of the emission source localization in the radio-detection experiments of extensive air showers

Ahmed Rebai^{a,*}, Tarek Salhi^b, Pascal Lautridou^{a,*}, Olivier Ravel^a

^a*SUBATECH IN2P3-CNRS/Université de Nantes/Ecole des Mines de Nantes, Nantes,
France*

^b*Ecole des Mines de Nantes, Nantes, France*

Abstract

Reconstruction of the curvatures of radio wavefronts of air showers initiated by ultra high energy cosmic rays is discussed based on minimization algorithms commonly used. We emphasize the importance of the convergence process induced by the minimization of a non-linear least squares function that affects the results in terms of degeneration of the solutions and bias. We derive a simple method to obtain a satisfactory estimate of the location of the main point of emission source, which mitigates the problems previously encountered.

Keywords: UHECR, radio-detection, antennas, non-convex analysis, optimization, ill-posed problem.

1. Introduction

The determination of the nature of the ultra-high energy cosmic rays (UHECR) is an old fundamental problem in cosmic rays studies. Numerous are the difficulties. New promising approaches could emerge from the use of the radio-detection method which exploits, through antennas, the radio signal that accompanies the development of the extensive air shower (EAS). Several experimental prototypes like CODALEMA [1] in France and LOPES [3] in Germany shown the feasibility and the potential of the method to reconstruct EAS parameters, as the arrival direction, the impact location at ground, the lateral distribution function of the electric field, or the primary particle energy [4, 5, 6, 7, 8]. However, the temporal radio wavefront characteristics remain still poorly determined [9, 10], although its knowledge could be consider as one of the first steps in retrieving information about the EAS itself. The importance of this information resides

*Corresponding authors

Email addresses: ahmed.rebai@subatech.in2p3.fr (Ahmed Rebai),
tareksalhi@gmail.com (Tarek Salhi), Pascal.Lautridou@subatech.in2p3.fr
(Pascal Lautridou), Olivier.Ravel@subatech.in2p3.fr (Olivier Ravel)

in its potential sensitivity to the nature of the primary particle, especially because the existence of a curvate radio wavefront (a spherical wavefront) could provide the location of the main point of the emission source, and possibly an estimation of X_{\max} , event by event. Indeed, the arrival timing being defined by the maximum amplitude of the radio signal, it is more likely linked to a limited portion of the longitudinal development of the shower (and so especially at the point of maximum) [11].

Moreover, the migration of present small scale radio-prototypes to large scale experiments spread over surfaces of several tens of 1000 km^2 using self-triggered antennas, is challenging. This technique is subjected to delicate limitations in regard to UHECR recognition, due to noises induced by human activities (high voltage power lines, electric transformers, cars, trains and planes) or by stormy weather conditions (lightning). Figure 1 shows a typical reconstruction of sources obtained with the CODALEMA experiment [12], by invoking a spherical wave minimization. Such patterns are also commonly observed in others radio experiments [14, 13]. In most of the cases, one of the striking results is that these emission sources are reconstructed with great inaccuracy, although they are fixed and although the number of measured events is high. By extension, a cosmic event being a single realization of the detected observables (arrival time and peak amplitude on each antenna), interpretation of such methods of reconstruction for the identification of a point source can become even more delicate, even using statistical approaches.

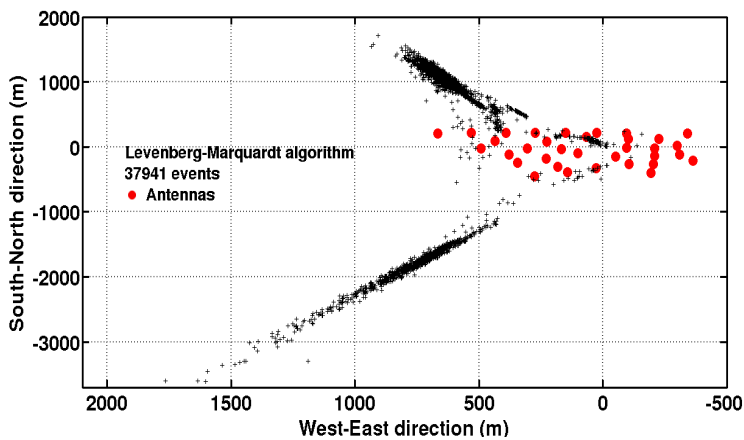


Figure 1: Typical result of reconstruction of two entropic emitters at ground, observed with the stand-alone stations of CODALEMA, through standard minimization algorithms. Despite the spreading of the reconstructed positions, these two transmitters are, in reality, two stationary point sources.

The commonly used technique relies on the minimization of an objective function which depends on the assumed shape of the wavefront, using the arrival times and locations of the antennas. The aim of this paper is to highlight

that the minimization of such an objective function, incorporating a spherical wave front, can be an ill-posed problem. We will show that it originates from strong dependencies of the convergence of the minimization algorithms with initial parameters, from the existence of degenerations of the solutions (half lines) which can trap most of the common algorithms, and from the existence of offsets (bias) in the reconstructed positions. Finally, by avoiding more complex estimates based on advanced statistical theories, we got to deduce a simple method to obtain a significant estimate of the source location. We compared the exact results with our numerical reconstructions performed on a test array.

2. Reconstruction with common algorithms

The performances of different algorithms has been tested using the simplest test array of antennas. Within the constraints imposed by the number of free parameters used for reconstruction, we choose an array of 5 antennas for which the antennas positions $\vec{r}_i = (x_i, y_i, z_i)$ are fixed (see Fig. 2) (this corresponds to a multiplicity of antennas similar to that sought at the detection threshold in current setups).

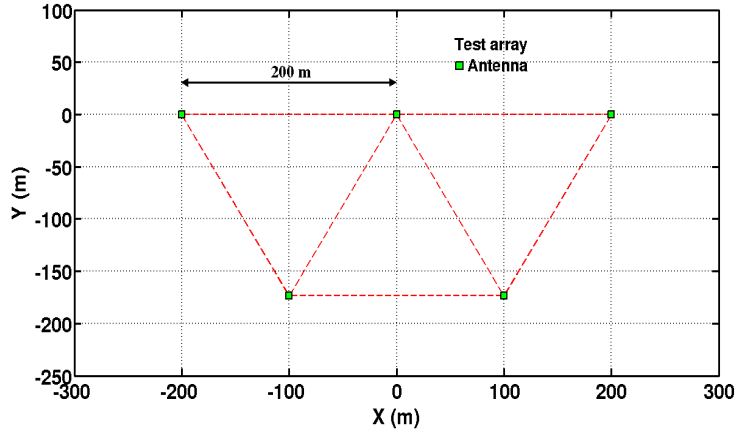


Figure 2: Scheme of the antenna array used for the simulations. The antenna location is taken from a uniform distribution of 1 m width.

A source S with a spatial position $\vec{r}_s = (x_s, y_s, z_s)$ is set at the desired value. Assuming t_s the unknown instant of the wave emission from S , c the wave velocity in the medium considered constant during the propagation, and assuming that the emitted wave is spherical, the reception time t_i on each antenna $i \in \{1, \dots, N\}$ can be written:

$$t_i = t_s + \frac{\sqrt{(x_i - x_s)^2 + (y_i - y_s)^2 + (z_i - z_s)^2}}{c} + G(0, \sigma_t)$$

where $G(0, \sigma_t)$ is the Gaussian probability density function centered to $t = 0$ and of standard deviation σ_t . This latter parameter stand for the the global time resolution, which depends as well on technological specifications of the apparatus than on analysis methods.

The theoretical predictions are compared to the reconstructions given by the different algorithms. The latter are setup in two steps. First, a planar adjustment is made, in order to pres-tress the region of the zenith angle θ and azimuth angle ϕ of the source arrival direction. It specifies a target region in this subset of the phase space, reducing the computing time of the search of the minimum of the objective function of the spherical emission. Reconstruction of the source location is achieved, choosing an objective-function that measures the agreement between the data and the model of the form, by calculating the difference between data and a theoretical model (in frequentist statistics, the objective-function is conventionally arranged so that small values represent close agreement):

$$f(\vec{r}_s, t_s) = \frac{1}{2} \sum_{i=1}^N \left[\|\vec{r}_s - \vec{r}_i\|^2 - (t_s - t_i)^2 \right]^2 \quad (1)$$

The partial terms $\|\vec{r}_s - \vec{r}_i\|^2 - (t_s - t_i)^2$ represents the difference between the square of the radius calculated using coordinates and the square of the radius calculated using wave propagation time for each of the N antennas. The functional f can be interpreted as the sum of squared errors. Intuitively the source positions \vec{r}_s at the instant t_s is one that minimizes this error.

In the context of this paper, we did not use genetic algorithms or multivariate analysis methods but we focused on three minimization algorithms, used extensively in statistical data analysis software of high energy physics[15, 16]: Simplex, Line-Search and Levenberg-Marquardt (see table 2). They can be found in many scientific libraries as the Optimization Toolbox in Matlab, the MPFIT in IDL and the library Minuit in Root that uses 2 algorithms Migrad and Simplex which are based respectively on a variable-metric linear search method with calculation of the objective function first derivative and a simple search method. For the present study, we have used with their default parameters.

We tested three time resolutions with times values took within $3\sigma_t$.

- $\sigma_t = 0 ns$ plays the role of the perfect theoretical detection and serves as reference;
- $\sigma_t = 3 ns$ reflects the optimum performances expected in the current state of the art;
- $\sigma_t = 10 ns$ stands for the timing resolution estimate of an experiment like CODALEMA [2].

For every source distance and temporal resolution, one million events were generated. Antenna location was taken in a uniform distribution of 1 m width. A blind search was simulated using uniform distribution of the initial r_s values

Minimization algorithms	Levenberg-Marquardt	Simplex	Line-Search
Libraries	lsqnonlin - MPFIT	fminsearch - SIMPLEX	MIGRAD - lsqcurvefit
Software	Optimization Toolbox Matlab - IDL	Optimization Toolbox Matlab - MINUIT-ROOT	Optimization Toolbox Matlab - MINUIT-ROOT
Method Principles	Gauss-Newton method combined with trust region method	Direct search method	Compute the step-size by optimizing the merit function $f(x + t.d)$
Used information	Compute gradient $(\nabla f)_k$ and an approximate hessian $(\nabla^2 f)_k$	No use of numerical or analytical gradients	$f(x + t.d, d)$ where d is a direction descent computed with gradient/hessian
Advantages / Disadvantages	Stabilize ill-conditioned Hessian matrix / time consuming and local minimum trap	No reliable information about parameter errors and correlations	Need initialization with another method, give the optimal step size for the optimization algorithm then reduce the complexity

Table 1: Summary of the different algorithms and methods used to minimize the objective-function. The second row indicates framework functions corresponding to each algorithm; third recalls the framework names. The key information used for optimization are recalled down, noting that a differentiable optimization algorithm (ie. non-probabilistic and non-heuristic) consists of building a sequence of points in the phase space as follows: $x_{k+1} = x_k + t_k.d_k$, and that it is ranked based on its calculation method of t_k and d_k parameters (see [17]).

from 0.1 km to 20 km . Typical results obtained with our simulations are presented in Figures 3 and 4. The summary of the reconstructed parameters is given in table 2.

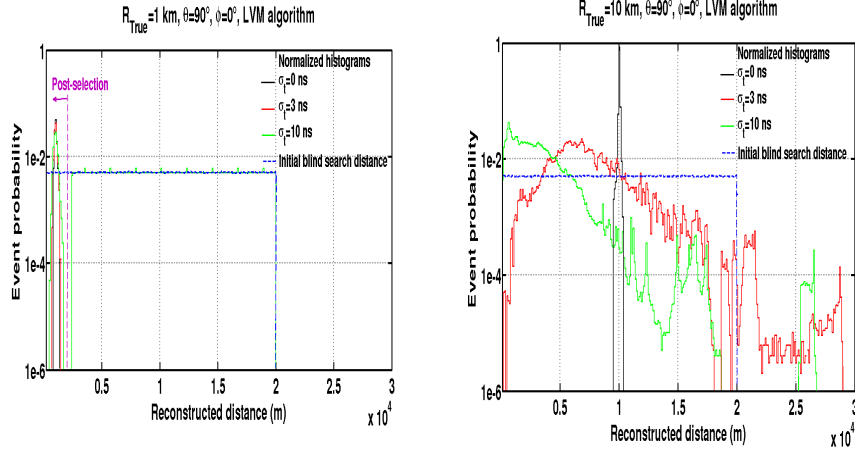


Figure 3: Results of the reconstruction of a source with a radius of curvature equal to 1 and 10 km with the LVM algorithm. For $R_{true} = 1 \text{ km}$, the effect of the blind search leads to non-convergence of the LVM algorithm, when initialization values are greater than $R_{true} = 1 \text{ km}$.

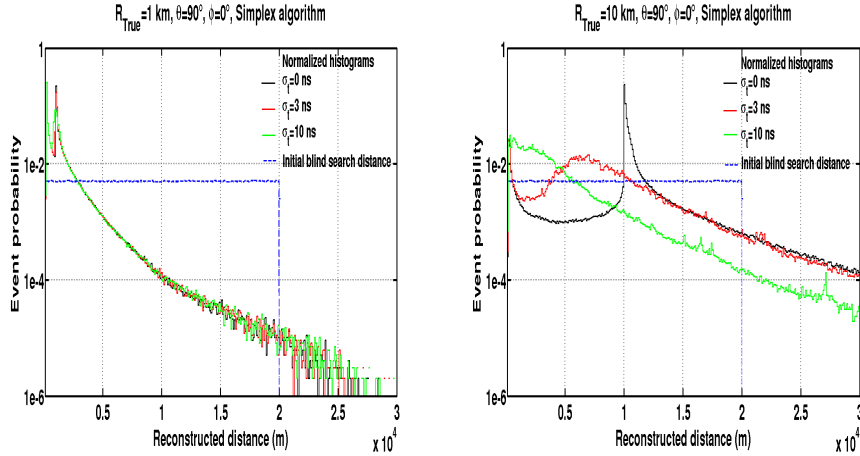


Figure 4: Results of the reconstruction of a source with a radius of curvature equal to 1 and 10 km with the Simplex algorithm.

Whatever the simulations samples (versus any source distances, arrival directions, time resolutions), (also with several detector configurations) and the three minimization algorithms, large spreads were generally observed for the source locations reconstructed. This suggests that the objective-function presents local minima. Moreover, the results depend strongly on initial conditions. All these

Reconstruction Results					
$\sigma_t (ns)$	$R_{true}(m)$	<i>Algorithms</i>	$R_{mean}(m)$	$R_{mode}(m)$	$\sigma^R(m)$
0	1000	Levenberg-Marquardt	(10071) 1002	(1081) 1081	(5763) 102
		Simplex	1198	1133	1477
	3000	Levenberg-Marquardt	(9960) 3082	(2998) 2998	(5781) 302
		Simplex	3134	3272	3437
	10000	Levenberg-Marquardt	9999	9997	56
		Simplex	10466	9929	5817
3	1000	Levenberg-Marquardt	(10071) 1003	(934) 934	(5763) 108
		Simplex	1199	168	1486
	3000	Levenberg-Marquardt	(9954) 3068	(2874) 2874	(5792) 495
		Simplex	3132	3010	3485
	10000	Levenberg-Marquardt	7174	6877	3021
		Simplex	8194	6479	6154
10	1000	Levenberg-Marquardt	(10068) 985	(964) 964	(5767) 175
		Simplex	1189	199	1507
	3000	Levenberg-Marquardt	(9703) 2238	(1620) 1620	(6125) 877
		Simplex	2760	2070	3703
	10000	Levenberg-Marquardt	2770	667	2305
		Simplex	3675	934	4048

Table 2: Summary of parameters reconstructed with different algorithms for several distances of source and several timing resolutions. On the Levenberg-Marquardt, the results in parentheses are those taking into account the flat portion of the resulting distribution (see Fig. 3). They are typical of initialization values which are starting too far from the actual source distance. The Line-Search method was ultimately rejected for this quantitative study, because results too dependent on the starting algorithm fixing the initial conditions.

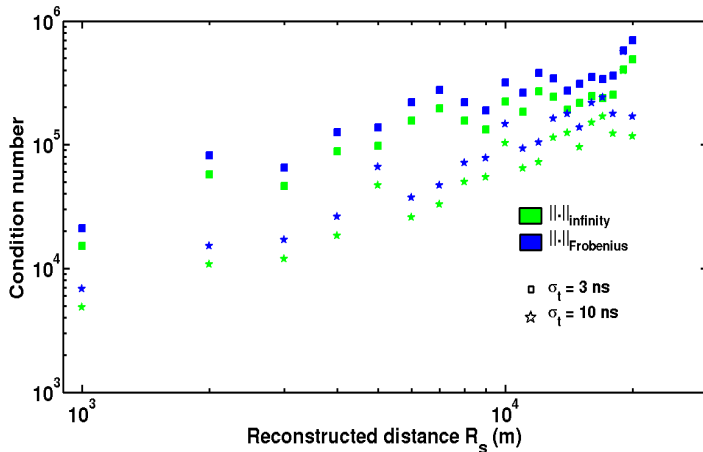


Figure 5: Condition numbers obtained using the formula $Cond(Q) = \|Q\| \cdot \|Q^{-1}\|$ with Q the Hessian matrix (see next section) as a function of the source distance and for different timing resolutions. The large values of conditioning suggest that we face an ill-posed problem.

phenomena may indicate that we are facing an ill-posed problem. Indeed, condition number calculations [19] (see Fig. 2), which measures the sensitivity of the solution to errors in the data (as the distance of the source, the timing resolution, etc.), indicate large values ($> 10^4$), when a well-posed problem should induce values close to 1.

To understand the observed source reconstruction patterns, we have undertaken to study the main features of this objective-function.

3. Study of the objective-function for the spherical emission

To estimate the source position $X_s = (\vec{r}_s, t_s)$ using the sequence of arrival t_i , the natural method is to formulate an unconstrained optimization problem of type a non-linear least square [17], starting from eq. 1. which can rewrite¹ (see the notations listed in table 3):

$$f(X_s) = \frac{1}{2} \sum_{i=1}^N \left[\|\vec{r}_s - \vec{r}_i\|_2^2 - (t_s^* - t_i^*)^2 \right]^2 = \frac{1}{2} \sum_{i=1}^N f_i^2(X_s) \quad (2)$$

Several properties of the objective-function f were studied: the coercive property to indicate the existence of at least one minima, the non-convexity to indicate the existence of several local minima, and the jacobian to locate

¹In practice of the minimization, it is usual to take into account errors on the measured parameters by putting them in the objective function denominator. In our theoretical study, it is assumed that the arrival times errors are the same for all the antennas ($\sigma_t = constant \forall i$). The present studied functional is generic and does not include errors, but as will see later, introduction of a multiplicative constant doesn't change the results of our study.

\vec{r}_s, \vec{r}_i : position of the source, position of the i^{th} antenna t_s, t_i : emission time of the signal, signal arrival time at the i^{th} antenna t_s^*, t_i^* : reduced time variables (ie. $t^* = c.t$) σ_i^t : time resolution on the i^{th} antenna X_s, X_i spacio-temporal position of the source, of the i^{th} antenna $\nabla f, \nabla^2 f$: first and second derivative of the objective function f $M = I_4 - 2E_{44} = \begin{bmatrix} 1 & 0 & 0 & 0 \\ 0 & 1 & 0 & 0 \\ 0 & 0 & 1 & 0 \\ 0 & 0 & 0 & -1 \end{bmatrix}$: second order tensor related to the Minkowski metric Q, L_i : quadratic and linear form $\langle . . \rangle$: inner product X^T : transpose of a vector or a matrix X

Table 3: List of notations

the critical points. (Bias study, which corresponds to a systematic shift of the estimator, is postponed to another contribution). In mathematical terms, this analysis amounts to:

- Estimate the limits of f to make evidence of critical points; obviously, the objective function f is positive, regular and coercive. Indeed, f tends to $+\infty$ when $\|X\| \rightarrow \pm\infty$, because it is a polynomial and contains positive square terms. So, f admits at least a minimum.
- Verify the second optimality condition: the convexity property of a function on a domain for a sufficiently regular function is equivalent to positive-definiteness character of its Hessian matrix.
- Solve the first optimality condition: $\nabla f(X_s) = 0$ (jacobian) to find the critical points.

3.1. Convexity property

Using $f_i(X_s) = (X_s - X_i)^T \cdot M \cdot (X_s - X_i)$ where M designates the *Minkowski* matrix and given $\nabla f_i(X_s) = 2 \cdot M \cdot (X_s - X_i)$, the f gradient function can be written (see appendix 1):

$$\frac{1}{2} \nabla f(X_s) = \left(\sum f_i(X_s) \right) M \cdot X_s - M \cdot \left(\sum f_i(X_s) X_i \right)$$

The Hessian matrix, which is the f second derivative can be written:

$$\nabla^2 f(X_s) = \sum \nabla f_i(X_s) \cdot \nabla f_i^T + \sum f_i \cdot \nabla^2 f_i$$

that becomes, replacing ∇f_i by its expression:

$$\nabla^2 f(X_s) = \left(\sum f_i(X_s) \right) \cdot M + 2M \cdot [N \cdot X_s \cdot X_s^T + \sum X_i X_i^T - X_s \left(\sum X_i \right)^T - \left(\sum X_i \right) X_s^T] \cdot M$$

Using a Taylor series expansion to order 2 (see appendix 1), an expanded form of the Hessian matrix, equivalent to the previous formula of the f second derivative, is:

$$\frac{1}{2}Q(X_s, X_i) = \begin{bmatrix} \sum_i K_i + 2\sum_i (x_s - x_i)^2 & 2\sum_i (x_s - x_i)(y_s - y_i) & 2\sum_i (x_s - x_i)(z_s - z_i) & 2\sum_i (x_s - x_i) \begin{pmatrix} t_i^* - t_s^* \\ t_i^* - t_s^* \end{pmatrix} \\ * & \sum_i K_i + 2\sum_i (y_s - y_i)^2 & 2\sum_i (y_s - y_i)(z_s - z_i) & 2\sum_i (y_s - y_i) \begin{pmatrix} t_i^* - t_s^* \\ t_i^* - t_s^* \end{pmatrix} \\ * & * & \sum_i K_i + 2\sum_i (z_s - z_i)^2 & 2\sum_i (z_s - z_i) \begin{pmatrix} t_i^* - t_s^* \\ t_i^* - t_s^* \end{pmatrix} \\ * & * & * & -\sum_i K_i + 2\sum_i \begin{pmatrix} t_i^* - t_s^* \\ t_i^* - t_s^* \end{pmatrix}^2 \end{bmatrix} \quad (3)$$

This latter allowed us to study the convexity of f (see appendix 1). Indeed, because its mathematical form is not appropriate for a direct use of the convexity definition, we have preferred to use the property of semi-positive-definiteness of the Hessian matrix. Our calculus lead to the conclusion that:

- Using the criterion of Sylvester [18] and the analysis of the principal minors of the Hessian matrix, we find that f is not convex on small domains, and thus is likely to exhibit several local minima, according to X_s and X_i . It is these minima, which induce convergence problems to the correct solution for the common minimization algorithms.

3.2. Critical points

The study of the first optimality condition (Jacobian = 0) gives the following system $\nabla f(X_s) = 0$ and allows finding the critical points and their phase-space distributions. Taking into account the following expression:

$$\frac{1}{2}\nabla f(\bar{X}_s) = (\sum f_i(\bar{X}_s))M.\bar{X}_s - M.(\sum f_i(\bar{X}_s)X_i)$$

we get the relation:

$$\bar{X}_s = \sum_{i=1}^N \frac{f_i(\bar{X}_s)}{\sum_j f_j(\bar{X}_s)} X_i \quad (4)$$

This formula looks like the traditional relationship of a barycenter. Thus, we interpret it in terms of the antennas positions barycenter and its weights. The weight function f_i expressing the space-time distance error between the position exact and calculated, the predominant direction will be the one presenting the greatest error between its exact and calculated position. The antennas of greatest weight will be those the closest to the source.

In practice (see appendix 2), because the analytical development of this optimality condition in a three-dimensional formulation is not practical, especially considering the nonlinear terms, we chose to study particular cases. We considered the case of a linear antennas array (1D) for which the optimality condition is easier to express with an emission source located in the same plane. This approach allows us to understand the origin of the observed degeneration which appears from the wave equation invariance by translation and by time reversal (known reversibility of the wave equation in theory of partial differential equations) and provides us a intuition of the overall solution. It also enlightens the importance of the position of the actual source relative to the antennas array

(the latter point is linked to the convex hull of the antenna array and is the object of the next section). Our study led to the following interpretations:

- The iso-barycenter of the antenna array (of the lit antennas for a given event) plays an important role in explaining the observed numerical degeneration. The nature of the critical points set determines the convergence of algorithms and therefore the reconstruction result.
- There are strong indications, in agreement with the experimental results and our calculations (for 1D geometry), that the critical points are distributed on a line connecting the barycenter of the lit antennas and the actual source location. We used this observation to construct an alternative method of locating the source (section 4).
- According to the source position relative to the antenna array, the reconstruction can lead to an ill-posed or well-posed problem, in the sense of J. Hadamard.

3.3. Convex hull

In the previous section we pointed that to face a well-posed problem (no degeneration in solution set), it was necessary to add constraints reflecting the propagation law in the medium, the causality constraints, and a condition linking the source location and the antenna array, the latter inducing the concept of convex hull of the array of antennas. From appendix 2, we also saw that analytically the critical points evidence could become very complex from the mathematical point of view. Therefore, we chose again an intuitive approach to characterize the convex hull, by exploring mathematically the case of a linear array with an emission source located in the same plane. This is the subject of the appendix 3.

The results extend to a 2D antenna array, illuminated by a source located anywhere at ground, arguing that it is possible to separate the array into sub-arrays arranged linearly. The superposition of all the convex segments of the sub-arrays leads then to conceptualize a final convex surface, built by all the peripheral antennas illuminated (see Figure 6).

The generalization of these results to real practical experience (with a source located anywhere in the sky) was guided by our experimental observations (performed through minimization algorithms) that provide a first idea of what happens. For this, we chose to directly calculate numerically the objective function for both general topologies: a source inside the antenna array (ie. and at ground level) and an external source to the antenna array (in the sky). As can be deduced from the results (see Figs. 7 and 8), for a surface antenna array, the convex hull is the surface defined by the antennas illuminated. (An extrapolation of reasoning to a 3D network (such as Ice Cube, ANTARES,...) should lead, this time, to the convex volume of the setup).

Our results suggest the following interpretations:

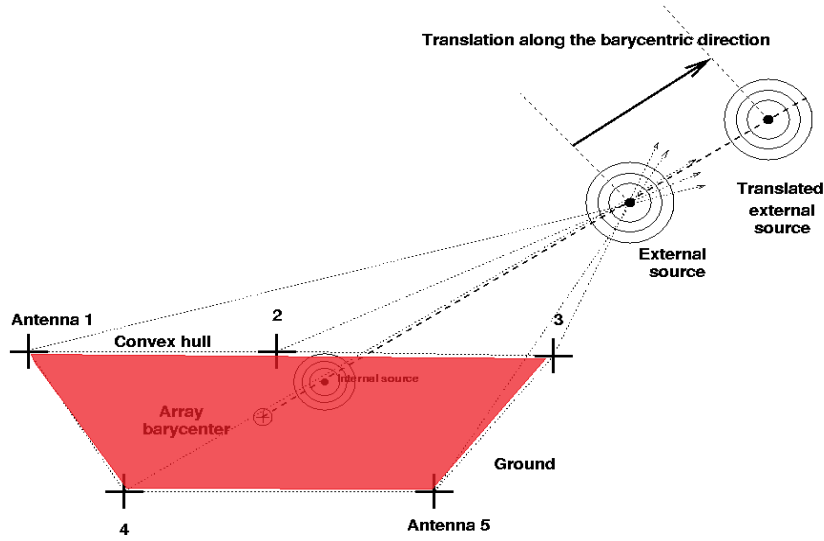


Figure 6: Scheme of the reconstruction problem of spherical waves for our testing array of antennas (2D), with a source located at ground. For this configuration, the convex hull becomes the surface depicted in red. The result is the same for a source in the sky.

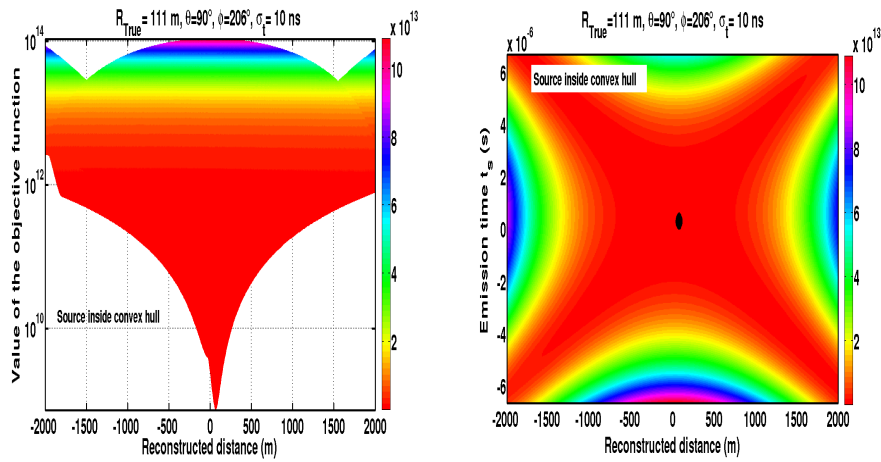


Figure 7: Plots of the objective-function versus R and versus the phase space (R, t) , in the case of our testing array (2D), for a source on the ground and located inside the convex surface of the antenna array. This configuration leads to a single solution. In this case the problem is well-posed.

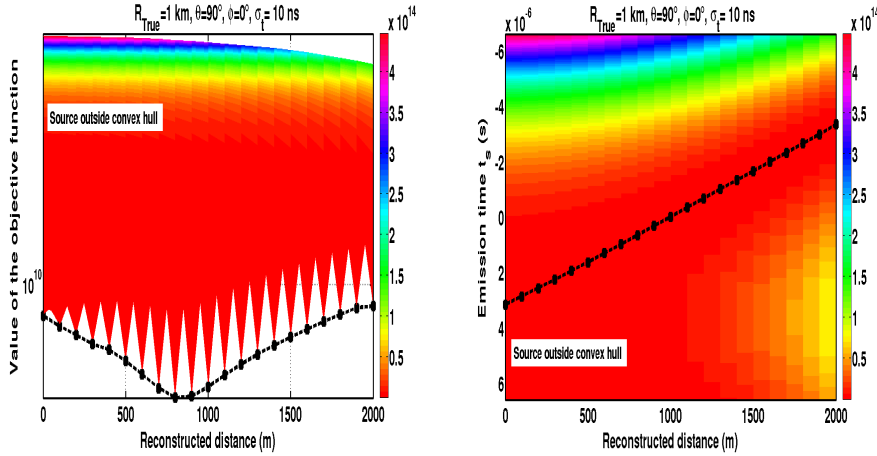


Figure 8: Plots of the objective-function versus R and versus the phase space (R, t) , in the case of our testing array (2D) for a source outside the convex hull. This configuration leads to multiple local minima. All minima are located on the line joining the antenna barycenter to the true source. In this case the problem is ill-posed.

- If the source is in the convex hull of the detector, the solution is unique. In contrast, the location of the source outside the convex hull of the detector, causes degeneration of solutions (multiple local minimums) regarding to the constrained optimization problem. The source position, outside or inside the array, affects the convergence of reconstruction algorithms.

4. Proposed method of reconstruction

Taking into account of the previous results, in order to avoid the trap of the local minima with common algorithms, we chose to compute directly the values of the objective function on a grid, using a subset of phase space in the vicinity of the solution a priori, and assuming that the minimum of the objective function correspond to the best estimate of the position of the source of emission. The input parameters are set from the planar fit, which provides both windows in θ and ϕ . By cons, this method, being based on the search of the minimum of the objective function using a grid calculation, the choice of the metric becomes crucial. On the zenith and azimuth angles, the metric can be adequately inferred from the value of the angular resolution obtained by the current detectors, or 0.1° for θ and ϕ . Looking at the space metrics, the latter can be inferred by considering the quantity $(c^2 \sigma_t^2)^2$, ie. around one meter. The direction-priori is given by the planar fit, while the quantity r_s is left free in the range $0.1 - 20 \text{ km}$ (the upper bound being determined by the value of the curvature exploitable, given the temporal resolutions currently available).

A typical result obtained with our method is presented in Fig. 9 and a summary of the reconstructed parameters is given in table 4 which have to be compared to those presented in the table 2.

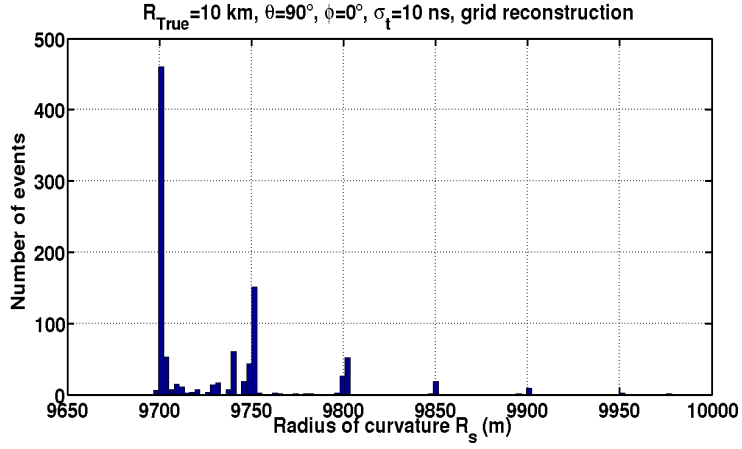


Figure 9: Histogram of the reconstruction of a source located at 10 km from the detector array, and using the grid method associated to the search of the global minimum for each event.

Reconstruction results				
$\sigma_t(ns)$	$R_{true}(m)$	$R_{mean}(m)$	$R_{mode}(m)$	$\sigma^R(m)$
0	1000	1000	1000	0
	3000	3000	3000	0
	10000	10000	10000	0
3	1000	1010	998	58
	3000	2964	2700	214
	10000	9806	9700	161
10	1000	987	902	150
	3000	2780	2700	149
	10000	9734	9700	50

Table 4: Summary of parameters reconstructed with our method for the same input values as given in table 3.

5. Conclusion

Experimental results indicated that the common methods of minimization of spherical wavefronts could induce a mis-localisation of the emission sources. In the current form of our objective function, a first elementary mathematical study indicates that the source localization method may lead to ill-posed problems, according to the actual source position. To overcome this difficulty, we developed a simple method, based on grid calculation of the objective function. This approach appears to provide, at worst, an estimate as good as for the common algorithms for locating the main point of the emission source, keeping in mind that this method is not optimal in the sense of optimization theories. However, further developments are without any doubt still necessary, maybe based on advanced statistical theories, like for instance by adding further information (as the signal amplitude or the functional of the radio lateral distribution). This could be achieved by trying a generalized objective function which includes these parameters. In addition, the interactions with other disciplines which face this problem could also provide tracks of work (especially regarding earth sciences which focus on technics of petroleum prospecting).

6. Appendix 1

6.1. Symbolic calculus

Keeping the same notation as in table 3, the objective function can be written:

$$f(X_s) = \frac{1}{2} \sum_{i=1}^N f_i^2(X_s)$$

with $f_i(X_s) = (X_s - X_i)^T \cdot M \cdot (X_s - X_i) = \|\vec{r}_s - \vec{r}_i\|^2 - (t_s^* - t_i^*)^2$.

The formula $\nabla f(X_s) = \sum f_i(X_s) \cdot \nabla f_i(X_s)$ is derived from the formula of a product derivation. Using the bi-linearity of the inner product, we show that $\nabla f_i(X_s) = 2M \cdot (X_s - X_i)$. By injecting this formula into the formula of ∇f , we obtain the following formula:

$$\begin{aligned} \nabla f(X_s) &= \sum f_i(X_s) \cdot \nabla f_i(X_s) \\ &= \sum f_i(X_s) \cdot 2M \cdot (X_s - X_i) \end{aligned}$$

It then leads to the following form:

$$\frac{1}{2} \nabla f(X_s) = \left(\sum f_i(X_s) \right) M \cdot X_s - M \cdot \left(\sum f_i(X_s) X_i \right)$$

With the same method, the second derivative matrix (Hessian matrix) is given by the following formula :

$$\nabla^2 f(X_s) = \sum \nabla f_i(X_s) \cdot \nabla f_i(X_s)^T + \sum f_i(X_s) \cdot \nabla^2 f_i(X_s)$$

By injecting in the previous formula the following formula of the second derivatives $\nabla^2 f_i(X_s) = 2M$ and by using the relation $(AB)^T = B^T A^T$, we get the following formula:

$$\begin{aligned} \nabla^2 f(X_s) &= \sum \nabla f_i(X_s) \cdot \nabla f_i(X_s)^T + \sum f_i(X_s) \cdot \nabla^2 f_i(X_s) \\ &= \sum 2M \cdot (X_s - X_i) \cdot (2M \cdot (X_s - X_i))^T + \sum f_i(X_s) \cdot 2M \\ &= 4M \cdot \left[\sum (X_s X_s^T - X_s X_i^T - X_i X_s^T + X_i X_i^T) \right] \cdot M + 2 \left(\sum f_i(X) \right) \cdot M \\ &= 4M \cdot \left[N X_s X_s^T + \sum X_i X_i^T - X_s \left(\sum X_i \right)^T - \left(\sum X_i \right) X_s^T \right] \cdot M + 2 \left(\sum f_i(X_s) \right) \cdot M \end{aligned}$$

Both relationships correspond to the end-calculus forms given in the 3rd section. These forms are easy to handle for symbolic calculus but not convenient for explicit calculation used for studying the convexity.

6.2. Taylor expansion and explicit calculus

An explicit form for the objective function first and second differential can be obtained using a Taylor expansion. Indeed, the function f is an element of $C^\infty(\mathbb{R}^4, \mathbb{R})$ ² and is therefore differentiable in the sense of *Fréchet*.

Let $X_s = (\vec{r}_s, t_s)^T$ be a fixed vector of \mathbb{R}^4 and $\vec{\varepsilon} = (\vec{h}, t^*)^T$ another vector of \mathbb{R}^4 . In order to simplify the calculus, we use the following notations :

$K_i = \|\vec{r}_s - \vec{r}_i\|_2^2 - (t_s - t_i)^2$ a constant term when setting the vector X_s ;

$L_i(\vec{\varepsilon}) = \langle \vec{r}_s - \vec{r}_i \mid \vec{h} \rangle - (t_s - t_i) \cdot t^*$ the linear form;

and $Q(\vec{h}, t^*) = \|\vec{h}\|_2^2 - t^{*2}$ the quadratic form.

The Taylor expansion leads to:

$$\begin{aligned} f(X_s + \vec{\varepsilon}) &= \frac{1}{2} \sum_i \left(\|\vec{r}_s + \vec{h} - \vec{r}_i\|_2^2 - (t_s + t^* - t_i)^2 \right) \\ &= \frac{1}{2} \sum_i \left(\langle \vec{r}_s + \vec{h} - \vec{r}_i \mid \vec{r}_s + \vec{h} - \vec{r}_i \rangle - (t_s + t^* - t_i)^2 \right) \\ &= \frac{1}{2} \sum_i \left(\|\vec{r}_s - \vec{r}_i\|_2^2 + \|\vec{h}\|_2^2 + 2 \langle \vec{r}_s - \vec{r}_i \mid \vec{h} \rangle - (t_s - t_i)^2 - t^{*2} - 2t^*(t_s - t_i) \right) \end{aligned}$$

Using the multinomial expansion, the function f can then be approximated by the second-order Taylor expansion following:

$$f(\vec{r}_s + \vec{h}, t_s + t^*) \approx \frac{1}{2} \sum_i K_i^2 + 2 \sum_i K_i \cdot L_i(\vec{h}, t^*) + 2 \sum_i L_i^2(\vec{h}, t^*) + \left(\sum_i K_i \right) \cdot Q(\vec{h}, t^*)$$

²The function is also an element of the algebra $\mathbb{R}[X_1, \dots, X_4]$

We identify from this formula:

the constant term $\frac{1}{2} \sum_i K_i^2$;

the linear term which is $\nabla f(X_s)^T \cdot \vec{\mathcal{E}} = \left[2 \cdot \sum_i K_i \begin{pmatrix} \vec{r}_s - \vec{r}_i \\ t_i^* - t_s^* \end{pmatrix} \right]^T \cdot \vec{\mathcal{E}}$ (the f first differential in (\vec{r}_s, t_s^*));
and the quadratic form at the point X_s :

$$\frac{1}{2} Q(X_s, X_i) = \begin{bmatrix} \sum_i K_i + 2 \sum_i (x_s - x_i)^2 & 2 \sum_i (x_s - x_i)(y_s - y_i) & 2 \sum_i (x_s - x_i)(z_s - z_i) & 2 \sum_i (x_s - x_i) \left(t_i^* - t_s^* \right) \\ * & \sum_i K_i + 2 \sum_i (y_s - y_i)^2 & 2 \sum_i (y_s - y_i)(z_s - z_i) & 2 \sum_i (y_s - y_i) \left(t_i^* - t_s^* \right) \\ * & * & \sum_i K_i + 2 \sum_i (z_s - z_i)^2 & 2 \sum_i (z_s - z_i) \left(t_i^* - t_s^* \right) \\ * & * & * & - \sum_i K_i + 2 \sum_i \left(t_i^* - t_s^* \right)^2 \end{bmatrix}$$

which is the f Hessian matrix in (\vec{r}_s, t_s^*) , or the second differential of f also denoted $\nabla^2 f(X_s, X_i)$. The use of * indicates that the coefficients above and below the diagonal are equal (*Schwarz Lemma*). The quadratic form represented by this matrix gives us the local second-order properties for the function f . To show that a critical point is a local minimum, it will suffice to verify that the Hessian matrix is definite positive in the vicinity of this point.

6.3. Convexity property

The convex analysis occupies a capital place in the problems of minimization. Indeed, an important theorem yet intuitive stated that if a convex function has a local minimum, it is automatically global. We will shows that the function f is not convex in \mathbb{R}^4 , i.e. that the Hessian matrix is non-positive definite.

Let $\nabla^2 f(X)$ the Hessian matrix, and let's suppose d a vector, since the function f is twice differentiable, using the Sylvester's criterion [18] to characterize the convexity of f , we can write the following equivalence:

f is convex \Leftrightarrow Hessian is positive semi-definite \Leftrightarrow All Hessian principal minors are just nonnegative

$$f \text{ is convex} \Leftrightarrow \forall d, \forall X, d^T \cdot \nabla^2 f(X) \cdot d \geq 0$$

So if we can find an element X and d such as $d^T \cdot \nabla^2 f(X) \cdot d < 0$, f will be non-positive definite. For this, it is sufficient to find a single negative principal minor to demonstrate the Hessian matrix is non-positive definite. The objective function f will present then several local minimums and will be thus locally non-convex.

So let Q the explicit expression of the Hessian and let us choose $d^T = (0001)$ then:

$$\begin{aligned} d^T \cdot \nabla^2 f(X) \cdot d &= (0 \ 0 \ 0 \ 1) \cdot Q(X_s, X_i) \cdot \begin{pmatrix} 0 \\ 0 \\ 0 \\ 1 \end{pmatrix} \\ &= - \sum_i K_i + 2 \sum_i (t_i^* - t_s^*)^2 \end{aligned}$$

which is represent the principal minor of order 4 of the Hessian.

For a family of fixed positions antennas and for a signal source with coordinates X_s such as $y_s = z_s = t_s^* = 0$, the negativity condition of the principal minor of order 4 can then written:

$$\sum_i (x_s - x_i)^2 > \sum_i (-y_i^2 - z_i^2 + 3t_i^{*2})$$

Now the left term tends to infinity when the source tends to infinity³. It is written in terms of limits,

$$\lim_{|x_s| \rightarrow +\infty} \sum_i (x_s - x_i)^2 = +\infty \Leftrightarrow \forall A > 0, \exists \eta > 0 / |x_s| > \eta \Rightarrow \sum_i (x_s - x_i)^2 > A$$

Taking a value $\sum_i (-y_i^2 - z_i^2 + 3t_i^{*2})$ of the constant A , it exist a real η and therefore a x_s such that $\sum_i (x_s - x_i)^2 > \sum_i (-y_i^2 - z_i^2 + 3t_i^{*2})$. We deduce that the function is not convex in the vicinity of this point. It suffices to take $d^T = (0 \ 0 \ 0 \ 1)$ and $x_s = \eta + 1$.

7. Appendix 2

7.1. Degeneration line for a linear antenna array

According to experimental data analysis and to our simulations (see Fig. 1 and 8), the results of the common minimization algorithms appear to fall on a half-line in the phase space (x, y, z) which we shall call the degeneration line, which is linked to the existence of local minima. We present the mathematical development in the case of a linear array using an analysis-synthesis method. Then we try to generalize results to the higher dimension cases.

Let suppose $X_s = (x_s, t_s^*)$ a critical point of f , ie. $\nabla f(X_s) = 0$, for a linear array, the minimization problem with constraints can written:

$$\left\{ \begin{array}{l} \arg \min f(x_s, t_s^*) = \frac{1}{2} \sum_{i=1}^N ((x_s - x_i)^2 - (t_s^* - t_i^*)^2) \quad 1 \leq i \leq N \\ \text{Propagation constraint : } |x_s - x_i| = |t_s^* - t_i^*| \\ \text{Causality constraint : } t_s^* < \min_i(t_i^*) \end{array} \right.$$

and Let suppose $L = \begin{pmatrix} L \\ L \end{pmatrix}$ so that $X_s - L$ is also a a solution of the minimization problem, ie. $\nabla f(X_s - L) = 0$)

The Jacobian of f is written as:

$$\vec{\nabla} f(x_s, t_s^*) = 2 \begin{pmatrix} \sum_i (x_s - x_i) \left((x_s - x_i)^2 - (t_s^* - t_i^*)^2 \right) \\ \sum_i (t_i^* - t_s^*) \left((x_s - x_i)^2 - (t_s^* - t_i^*)^2 \right) \end{pmatrix}$$

³We say that the function is *coercive*

If X_s being a critical point, this leads to two equations:

$$\begin{cases} \sum_i (x_s - x_i) \left((x_s - x_i)^2 - (t_s^* - t_i^*)^2 \right) = 0 & (1) \\ \sum_i (t_i^* - t_s^*) \left((x_s - x_i)^2 - (t_s^* - t_i^*)^2 \right) = 0 & (2) \end{cases}$$

Assuming that $X_s - L$ being also a critical point, this leads to two equations:

$$\begin{cases} \sum_i (x_s - x_i - L) \left((x_s - x_i - L)^2 - (t_s^* - t_i^* - L)^2 \right) = 0 & (3) \\ \sum_i (t_i^* - t_s^* + L) \left((x_s - x_i - L)^2 - (t_s^* - t_i^* - L)^2 \right) = 0 & (4) \end{cases}$$

By developing the equation (3) and by using the equation (1), then:

$$\begin{aligned} (3) \Rightarrow \sum_i (x_s - x_i) \left[(x_s - x_i)^2 - (t_s^* - t_i^*)^2 - 2L[(x_s - x_i) - (t_s^* - t_i^*)] \right] - L \sum_i (x_s - x_i)^2 - (t_s^* - t_i^*)^2 \\ \dots + 2L^2 \sum_i [(x_s - x_i) - (t_s^* - t_i^*)] = 0 \\ \Rightarrow -L \sum_i (x_s - x_i)^2 + L^2 \sum_i [(x_s - x_i) - (t_s^* - t_i^*)] - L \sum_i (x_s - x_i)^2 - (t_s^* - t_i^*)^2 \\ \dots + L \sum_i (x_s - x_i) (t_s^* - t_i^*) = 0 \end{aligned}$$

The set of constraints requires that the term $\sum_i (x_s - x_i)^2 - (t_s^* - t_i^*)^2$ is null.

We get the simplified equation:

$$L \sum_i (x_s - x_i) - (t_s^* - t_i^*) = \sum_i (x_s - x_i) ((x_s - x_i) - (t_s^* - t_i^*))$$

In the cases where $x_s - x_i < 0$ for all i , the set of constraints is equivalent to $(x_s - x_i) - (t_s^* - t_i^*) = 0$. Thus, if one assumes that $x_s - x_i < 0$ for all i , i.e that the source is outside the array convex hull (a segment), we find that previous implications are equivalences and thus that equation (3) is verified. Operating in the same manner for the equation (4), we obtain the following equations:

$$\begin{aligned} (4) \Rightarrow \sum_i (t_i^* - t_s^*) \left[(x_s - x_i)^2 - (t_s^* - t_i^*)^2 - 2L[(x_s - x_i) - (t_s^* - t_i^*)] \right] + L \sum_i (x_s - x_i)^2 - (t_s^* - t_i^*)^2 \\ \dots - 2L^2 \sum_i [(x_s - x_i) - (t_s^* - t_i^*)] = 0 \\ \Rightarrow -2L \sum_i (t_i^* - t_s^*) (x_s - x_i) - 2L \sum_i (t_i^* - t_s^*)^2 + L \sum_i (x_s - x_i)^2 - (t_s^* - t_i^*)^2 \end{aligned}$$

$$\dots - 2L^2 \sum_i (x_s - x_i) - (t_s^* - t_i^*) = 0$$

Using the set of constraints as above, we obtain the following equation:

$$L \sum_i (x_s - x_i) - (t_s^* - t_i^*) = \sum_i (t_i^* - t_s^*) ((x_s - x_i) - (t_s^* - t_i^*))$$

The same analysis as above gives us the condition that the source is out of the antennas convex hull. This degeneration is an important point because it determines the convergence of minimization algorithms. In this case the problem of the reconstruction is ill-posed.

The generalization of the previous calculation to higher dimensions is more delicate, insofar as there are infinitely many directions in which the source can move. The idea now is to translate the source, from its position \vec{r}_s , simultaneously in all directions $\vec{r}_s - \vec{r}_i$ and with the same distances. We define the unit vector on the direction source-antenna. It will be noted: $\vec{e}_i = \frac{\vec{r}_s - \vec{r}_i}{\|\vec{r}_s - \vec{r}_i\|_2}$. The translation spatial direction thus defined, is given by the vector $\vec{L} = \sum_i \vec{e}_i = \sum_i \frac{\vec{r}_s - \vec{r}_i}{\|\vec{r}_s - \vec{r}_i\|_2} = -\sum_i \frac{\vec{r}_i}{\|\vec{r}_s - \vec{r}_i\|_2} + \left(\sum_i \frac{1}{\|\vec{r}_s - \vec{r}_i\|_2} \right) \vec{r}_s$. Considering the reduced temporal variables, the wave required delay to traverse the distance induced by the translation $\|\vec{L}\|$. Let V the vector of coordinates $V = \left(\vec{L}, \|\vec{L}\| \right)^T$. We write the first order optimality condition for the vector of \mathbb{R}^4 : $X_s - V$:

$$\nabla f(X_s - V) = \left(\sum f_i(X_s - V) \right) \cdot M \cdot (X_s - V) - M \cdot \left(\sum f_i(X_s - V) \cdot X_i \right)$$

By introducing the condition $\nabla f(X_s) = 0$ which implies that:

$$\left(\sum f_i(X_s) \right) \cdot M \cdot X_s - M \cdot \left(\sum f_i(X_s) X_i \right) = 0$$

we obtain:

$$\begin{aligned} \nabla f(X_s - V) = & N (V^T \cdot M \cdot V) \cdot M \cdot \left[X_s - V - \frac{1}{N} \sum_i X_i \right] \\ & 2M \left(\sum (X_s - X_i)^T M \cdot V \cdot \vec{X}_i \right) - 2 \left(\sum (X_s - X_i)^T M \cdot V \right) \cdot M \cdot (X_s - V) \\ & - \left(\sum f_i(X_s) \right) \cdot M \cdot V \end{aligned}$$

According to the imposed form of the vector \vec{V} , then:

$$V^T \cdot M \cdot V = \left(\vec{L} \|\vec{L}\|_2 \right) M \left(\vec{L} \|\vec{L}\|_2 \right)^T = 0$$

It remains then the following expression:

$$\begin{aligned} \nabla f(X_s - V) = & 2M \left(\sum (X_s - X_i)^T M \cdot V \cdot X_i \right) - 2 \left(\sum (X_s - X_i)^T M \cdot V \right) \cdot M \cdot (X_s - V) \\ & - \left(\sum f_i(X_s) \right) \cdot M \cdot V \end{aligned}$$

The resolution of this equation should lead to an analytical expression for the topology of critical points. We failed to develop it, but we can already see that the explicit development leads to cross terms that will make simplifications difficult. Therefore, we have tried again an intuitive approach based on the numerical simulations presented section 3.3.

8. Appendix 3

8.1. Convex hull for a linear antenna array

Let us consider the sub-array of the 3 aligned upper antennas presented in Fig. 2). The figure 10 shows the physical principle of the reconstruction of the source.

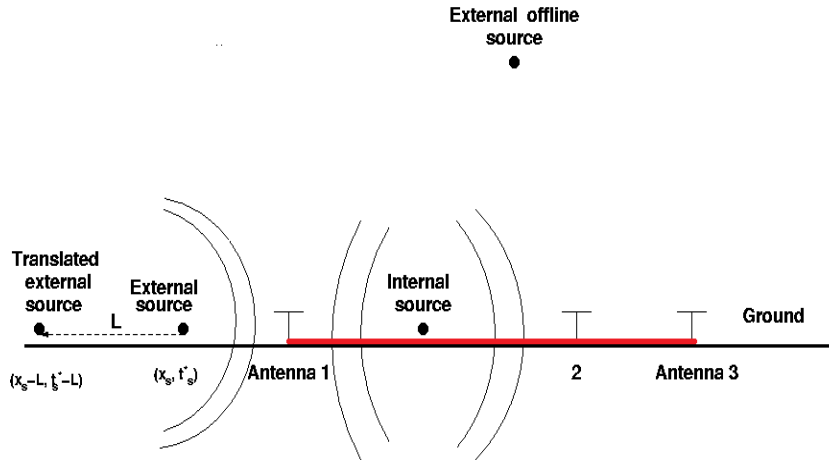


Figure 10: Scheme of the reconstruction problem of spherical waves for a 1D array of antennas. For this configuration, the convex hull is the segment shown in red.

Three situations must be considered:

- the source located inside the array;
- the source located outside the array but on the detector axis;
- the source located outside this main axis. The latter corresponds to the typical problems encountered with of the man-made emitters located on the ground.

The first situation leads to 2 half-lines cutting each other in a single point: the solution is unique (Figure 11) and the localization problem is well-posed. The source is unique and inside the line segment linking the nearest antennas to the source. This segment correspond to the convex hull within this geometry. We can also note that only the two antennas flanking the source then play a role in its localization. The problem writes:

$$\left\{ \begin{array}{l} \arg \min f(x_s, t_s^*) = \frac{1}{2} \sum_{i=1}^N ((x_s - x_i)^2 - (t_s^* - t_i^*)^2)^2 \\ \text{Propagation constraint : } |x_s - x_i| = |t_s^* - t_i^*| \\ \text{Causality constraint : } t_s^* < \min_i(t_i^*) \end{array} \right.$$

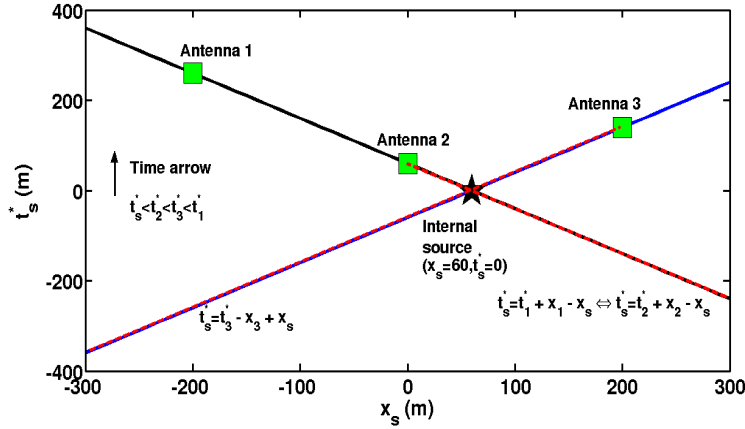


Figure 11: Phase space representation in the case of a linear array of three antennas (shown as green squares located at $x_1 = -200$ m, $x_2 = 0$ m, $x_3 = 200$ m). The source is located at $x_s = 60$ m when the instant of the emission is taken as the time origin ($t_s = 0$ s). Because the source is outside this sub-array, the constraints on the positions of antenna 1 and 2 lead to the same equation $t_s = 60 - x_s$ (black line). Equation for the antenna 3 (blue line) leads to $t_s = -60 + x_s$. The causality conditions restrict the initial lines to two half-lines (red lines). The source location (black star) is at the intercept of the both half-lines.

About the source on-axis, but outside the convex hull, the arrival times between the antennas, are no longer related to the source position, but to their locations. Whatever their positions, the time differences remain constant (for equally spaced antennas). It becomes impossible to distinguish between two different shifted sources by any length. The only relevant information lies in the direction of propagation of the wave (see figure 12). This result appears by a degeneration of solutions because all points located on the half-line starting from the first tagged antenna are solutions of the problem which is ill-posed. The source is outside the convex hull of the antenna array.

On the configuration where source located outside this antenna axis (problem in two dimensions), the solving starts with:

$$\left\{ \begin{array}{l} \arg \min f(x_s, y_s, t_s^*) = \frac{1}{2} \sum_{i=1}^N ((x_s - x_i)^2 + y_s^2 - (t_s^* - t_i^*)^2)^2 \\ \text{Propagation constraint : } (x_s - x_i)^2 + y_s^2 = (t_s^* - t_i^*)^2 \\ \text{Causality constraint : } t_s^* < \min_i(t_i^*) \end{array} \right.$$

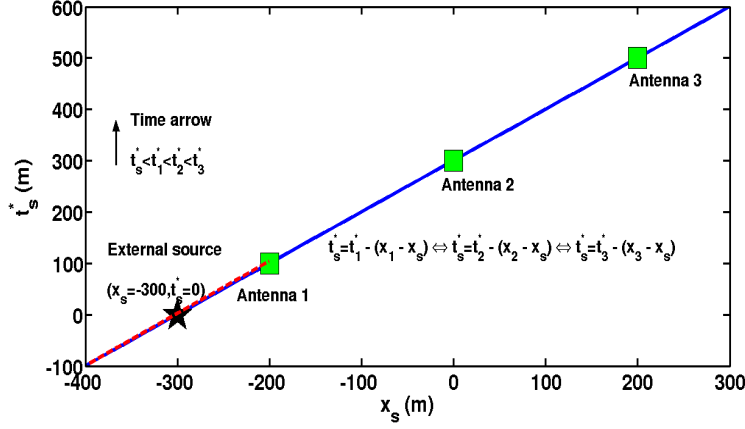


Figure 12: Same as figure 11 but for an on-axis source outside the linear array of three antennas. The whole constraints lead the same equation $t_s^* = 60 - x_s$. All points belonging to the lower half-line are solutions of the source localization problem (red dashed line), which becomes, in this case, ill-posed, and creates the degenerations.

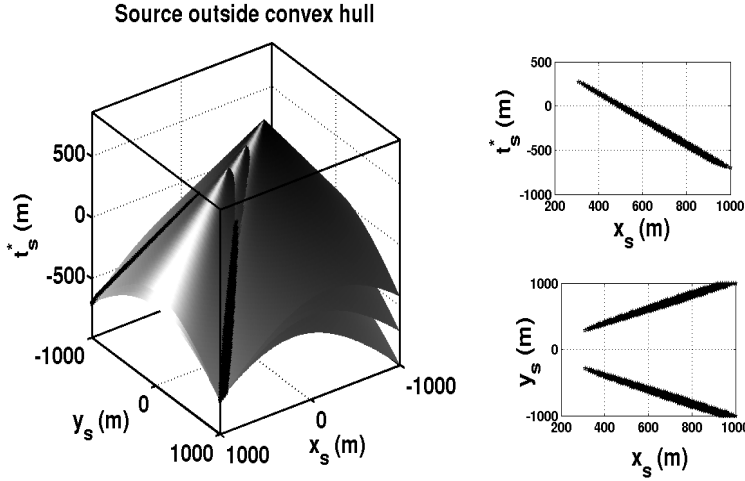


Figure 13: Reconstruction problem of spherical waves for a 1D array of antennas with the source outside the convex hull. The local minima are located at the intersection of the cones.

The constraint set reduces the problem of characterization of critical points to the search of the half-cones intersections induced by each antenna, in the 3 dimensional phase space (x, y, t) and which presents a great similarity of constraints with the light cone used in special relativity (Fig. 13). Intersection of the half-cones, two to two, induces multiple critical points which are local minima.

References

- [1] D. Ardouin, et al., Radio-detection signature of high-energy cosmic rays by the CODALEMA experiment, *Nucl. Instr. and Meth. A* 555 (2005) 148.
- [2] P. Lautridou for the CODALEMA Collaboration, Toward the autonomous radio-detection of ultra-high energy cosmic rays with CODALEMA, Proc. of the 3rd Roma International Conference on Atroparticle Physics, Roma 2011, *Nucl. Instr. and Meth. 2012*: DOI 10.1016/j.nima.2012.01.013.
- [3] H. Falcke, et al., Detection and imaging of atmospheric radio flashes from cosmic ray air showers, 2005, *Nature* 435, 313-316.
- [4] W. D. Apel et al. , Lateral distribution of the radio signal in extensive air showers measured with LOPES, *Astropart. Phys.*, (32) 2010, 294.
- [5] D. Ardouin et al., Geomagnetic origin of the radio emission from cosmic ray induced air showers observed by CODALEMA, *Astropart. Phys.*, 31 (2009), 294.
- [6] V. Marin for the CODALEMA collaboration, Charge excess signature in the CODALEMA data, Interpretation with SELFAS2, Proc. of the 32nd ICRC, Beijing, 2011.
- [7] A. Horneffer, et al., Primary particle energy calibration of the EAS radio pulse height, Proc. of the 30th ICRC, Mérida 2007, Vol 4. (HE part 1), 83-86.
- [8] P. Lautridou for the CODALEMA Collaboration, Results of the radio-detection experiment CODALEMA, *Nucl. Instr. and Meth. , A* 604, (2009) S13–S19.
- [9] S. Lafebre, et al., Prospects for determining air shower characteristics through geo-synchrotron emission arrival times, *Astropart. Phys.* 34 (2010) 12-17
- [10] D. Ardouin et al. (Trend collaboration): First detection of extensive air showers by the TREND self-triggering radio experiment, *Astropart.*, (34) 2011, 717.
- [11] V. Marin et al., Simulation of radio emission from cosmic ray air shower with SELFAS2, *Astropart. Phys.* 35 (2012) 733.
- [12] P. Lautridou for the CODALEMA collaboration, Some possible interpretations from data of the CODALEMA experiment, Proc. of the 5th international workshop on Acoustic and Radio EeV Neutrino Detection Activities (ARENA 2012), Erlangen 2012.

- [13] K. Weidenhaupt for the Pierre Auger Collaboration, The Auger Engineering Radio Array, XIV Vulcano Workshop, May 28 - June 2, 2012, Sicily, Italy, to be published in *Acta Polytechnica* 2013 Vol. 53 N. 1. (ed. by F. Giovannelli and G. Mannocchi).
- [14] L. Mohrmann, Measurement of Radio Emission from Cosmic Ray induced Air Showers at the Pierre Auger Observatory with a Spherical Wave Reconstruction, Masterarbeit in Physik, Univ. of Aachen 2011.
- [15] F. James and M. Roos, MINUIT - A system for function minimization and analysis of the parameter errors and correlations, *Computer Physics Communications* 10 (1975), 343-367.
- [16] C. B. Markwardt, Non-linear Least Squares Fitting in IDL with MPFIT, 2009, arXiv.org/astro-ph/arXiv:0902.2850.
- [17] J. F. Bonnans et al. , *Numerical Optimization: Theoretical and Practical Aspects*, Springer-Verlag, Universitext, (second ed.) 2003.
- [18] R. A. Horn, C. R. Johnson, *Matrix Analysis*, Cambridge University Press, (first ed. 1985) 1999.
- [19] F. Delprat-Jannaud and P. Lailly, Ill-Posed and Well-Posed Formulation of the Reflection Travel Time Tomography Problem, *J. of Geophysical Research*, vol. 98, No. B4, p. 6589, April 10, 1993.